An easy co-casting method to synthesize mesostructured carbon composites with high magnetic separability and acid resistance†

Limin Guo, Shaozhong Zeng, Jiangtian Li, Fangming Cui, Xiangzhi Cui, Wenbo Bu and Jianlin Shi*

Received (in Victoria, Australia) 3rd April 2009, Accepted 26th May 2009
First published as an Advance Article on the web 24th June 2009
DOI: 10.1039/b906776k

Magnetic mesoporous carbon composites with high surface areas and narrow mesopore size distributions were directly replicated from SBA-15 by a simple co-casting method and the amount of incorporated magnetic particles and saturation magnetization value can be easily tuned by changing the added amount of iron source during synthesis. Furthermore, the magnetic mesoporous carbon composites show good acid resistance due to a carbon shell coating structure around the magnetic particles, which is spontaneously formed during the replication process of the mesoporous carbon composites. The characteristics of the as-synthesized magnetic mesoporous carbon composites were examined by X-ray diffraction, N_2 sorption, transmission electron microscopy (TEM), Mössbauer spectroscopy and vibrating-sample magnetometry.

1. Introduction

Mesoporous materials, with a variety of desired properties, are extensively investigated for their potential use as absorbents, catalysts, and supports in the chemical and petrochemical industries.[1–8] Great progresses have been made in developing novel mesoporous structures and morphologies during the past two decades, both through continued improvement of existing fabrication strategies and the development and introduction of new synthetic techniques.[9–14] One of very interesting mesoporous materials is ordered mesoporous carbons (OMCs),[15–17] which could be obtained either by nanocasting from ordered mesoporous silica as a hard template[18–21] or by direct soft-template synthesis procedures.[22,23] OMCs are suitable for many different applications due to their combined advantages of chemical inertness, biocompatibility, thermal stability, many mesostructural candidate types and high surface areas. There have been many investigations to develop the techniques of OMC surface modification for applications in separation, catalysis and electronics, and some excellent performances of OMCs have been found and studied as adsorbents and catalyst supports. OMCs as adsorbents showed a larger adsorption amount of phenol and its derivatives,[24] vitamin E,[25a] L-histidine, lysozyme,[25b] protein[25c] and bulky dyes.[26] However, the OMCs are often used in liquid-phase processes and are difficult to separate, and thus magnetic separation is an attractive way for filtration or centrifugation applications and therefore has been high on the 'wish list' in adsorption and catalysis for a long time.[27,28] A great attention and many efforts have been paid for synthesizing magnetically separable porous carbons.[29–33] Nevertheless, the existing synthetic strategies still suffer from problems for the as-prepared mesoporous carbon composites to be widely used. First, some synthetic procedures introduced nanosized magnetic particles into the mesopore channels, which would lead to substantial blocking of the pore channels by magnetic particles and rather low magnetic strength due to the very small size of the particles; Second, in some as-synthesized magnetic mesoporous carbons, magnetic particles are on the outside of the mesoporous carbon and therefore easily subject to oxidation in air or dissolution in acid. Third, most of the existing synthetic procedures are time-consuming, high-cost and complicated for obtaining the required materials, and the yield is relatively low. Despite these limitations, hindering practical applications, however, all of these previous works mentioned above indeed gave us some important hints to develop an economical, versatile and high yield synthetic route to magnetic mesoporous carbons.

Herein, we develop an easy route in this report to fabricate magnetically separable mesoporous carbon composites, which combines the advantages of high and tunable magnetic strength, high chemical resistance against acid attack due to the protection by a carbon layer coating, and high yield due to the simplicity of the synthetic procedures. Also in this scheme, the iron source was used as both the catalyst for furfuryl alcohol polymerization and as the magnetic particle precursor. The carbonization process was carefully controlled leading to the formation of mesoporous carbon and the iron precursor was simultaneously reduced into magnetic particles and the resultant composite is a magnetic mesoporous carbon composite possessing a structure of carbon-coated magnetic particles integrated onto the mesoporous carbon particle surface. Such a structure has been pursued and synthesized through a relatively complicated strategy,[29] however, in the present

State Key Laboratory of High Performance Ceramics and Superfine Microstructure, Shanghai Institute of Ceramics, Chinese Academy of Sciences, 1295 Ding-xi Road, Shanghai 200050, People's Republic of China. E-mail: jlshi@sunm.shcnc.ac.cn; Fax: +86-21-52413122; Tel: +86-21-52412714

† Electronic supplementary information (ESI) available: Fig. S1: Mössbauer spectrum of R-3-850 at room temperature. Fig. S2: Magnetization curves of the magnetic mesoporous carbon composites MC-1-750 and MC-2-750. Fig. S3: Magnetization curves of the magnetic mesoporous carbon composites MC-3-750 and MC-4-750. See DOI: 10.1039/b906776k

report, a very similar structure has been successfully obtained by an easy co-casting method through the co-introduction of carbon and iron source into the pore channels of a silica template, and the present route shows tunable magnetization intensity and high chemical stability.

2. Experimental

2.1 Chemicals

Poly(ethylene oxide)–poly(propylene oxide)–poly(ethylene oxide) triblock copolymer Pluronic P123 ($EO_{20}PO_{70}EO_{20}$) was purchased from BASF Chemical Company. Other chemicals were purchased from Sinopharm Chemical Reagent Corporation. All chemicals were used as received without any further purification.

2.2 Preparation of magnetic mesoporous carbon composites

The mesoporous silica template SBA-15 was synthesized according to a previously reported method.[11a] The magnetic mesoporous carbon composites were synthesized using SBA-15 as the hard template, $Fe(NO_3)_3{\cdot}9H_2O$ as iron source and catalyst, and furfuryl alcohol as the carbon source. Typically, 1.5 mL furfuryl alcohol and a given mass of $Fe(NO_3)_3{\cdot}9H_2O$ were dissolved in 15 mL ethanol. This solution was incorporated into 1.2 g SBA-15 by a wetness impregnation technique. After evaporating ethanol and polymerizing furfuryl alcohol at 80 °C for 12 h, the composite was thermally treated in nitrogen at 750 °C for 4 h to carbonize the polyfurfuryl alcohol. The silica template in the composite was removed by twice washing with hot 2 M NaOH solution. Then the obtained template-free magnetic mesoporous carbon composite was collected by a magnet, washed with water and absolute ethanol, and dried at 80 °C overnight. A series of samples were synthesized to tune the magnetic property and mesostructural parameters of the carbon composites by changing the added amount of $Fe(NO_3)_3{\cdot}9H_2O$. Samples MC-1-750, MC-2-750, MC-3-750 and MC-4-750 correspond to added amounts of 0.54, 1.18, 2.04 and 6.41 g of $Fe(NO_3)_3{\cdot}9H_2O$, respectively, and carbonization temperature of 750 °C. Several reference samples, which were denoted as R-3-700, R-3-800 and R-3-850, were synthesized to study the influence of carbonization temperature on the composite (700, 800 and 850 °C, respectively).

2.3 Acid resistance measurement of as-prepared magnetic mesoporous carbon composite

0.2 g of MC-2-750 were stored in 200 mL of HCl solution (pH = 1) for ten days. After filtration, washing with distilled water and ethanol, and drying, the acid-treated sample was denoted as MC-2-750-a.

2.4 Characterization

Powder XRD patterns were recorded on a Rigaku D/Max-2550V diffractometer using Cu-Kα radiation (40 kV and 40 mA). The scanning rate was 0.6 and 6° min^{-1} for low- and high-angle measurements, respectively. Nitrogen sorption isotherms at −196 °C were measured on a Micromeritics Tristar 3000 system. Before measurement, samples were pre-treated at 373 K for 12 h under nitrogen. The specific surface area and the pore size distribution were calculated by the BET (Brunauer–Emmett–Teller) equation and Barrett–Joyner–Halenda (BJH) method, respectively. TEM images were obtained on a JEM-2010 electron microscope operated at 200 kV. A vibrating-sample magnetometer (PPMS Model 6000 Quantum Design) was used to study the magnetic properties. ^{57}Fe Mössbauer spectra were recorded on a Wissel spectrometer in the constant acceleration mode, using a ^{57}Co (Pd) source.

3. Results and discussion

3.1 Structural characteristics of the magnetic mesoporous carbon composites

Fig. 1 illustrates the schematic procedure used in this work for synthesizing the magnetic mesoporous carbon composites. In step 1, after removing the surfactant template from mesoporous silica by calcination, an ethanol solution of furfuryl alcohol and iron nitrate was introduced into the mesoporous templates and then polymerized. Here, the polymerization was catalyzed by the acid sites of co-introduced iron nitrate.[32] In step 2, polyfurfuryl alcohol was carbonized under N_2 at high temperature. In this process, the cross-linked polymer matrix was converted into a carbon compact and iron nitrate mixture was decomposed/reduced to magnetic particles accompanying the carbonization process. After the silica template was removed by hot 2 M NaOH aqueous solution, the magnetic mesoporous carbon composites were obtained (step 3). Interestingly, most magnetic particles (as revealed by TEM imaging (see Fig. 3 below), existed on the outer surface of the mesoporous carbon particles and carbon shells were coated on the magnetic particles so integrating them onto the mesoporous carbon matrix. Such a coating structure was obtained due to our co-casting approach in which a small amount of iron

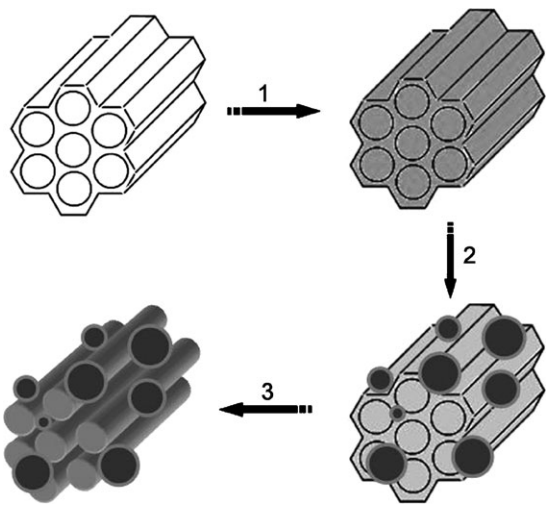

Fig. 1 Schematic illustration of the preparation of magnetic mesoporous carbon composites: (1) the mixed ethanol solution of furfuryl alcohol and iron nitrate was introduced into the mesoporous templates and polymerization; (2) carbonization of the polyfurfuryl alcohol, iron nitrate decomposition and spontaneous reduction into magnetic particles along with the carbonization process; (3) removal of the silica template.

source was highly dispersed within the carbon source during co-casting, and during polymerization and carbonization, the magnetic particles formed within the polyfurfuryl alcohol matrix and were finally covered by a carbon shell layer and integrated onto the carbon surface.

Fig. 2 shows XRD patterns of the magnetic mesoporous carbon composites with different magnetic particle loading levels under the same carbonization temperature (750 °C). The magnetic mesoporous carbon composites of MC-1-750 exhibit three reflections in the 2θ range between 1 and 2.5°, while no low-angle peaks for other samples were detected, which means that the ordered mesostructure has been destroyed along with the increase of the magnetic content. The high-angle XRD patterns of magnetic mesoporous carbon composites show characteristic diffraction peaks of α-Fe, magnetic iron oxide (Fe_3O_4 or γ-Fe_2O_3). Here, the magnetic iron oxide is confirmed by room-temperature Mössbauer spectroscopy to be Fe_3O_4. Strong and sharp diffraction peaks of α-Fe are found in MC-2-750, MC-3-750 and MC-4-750, as compared with those of Fe_3O_4, so α-Fe is the main magnetic source of the magnetic carbon composites.

Representative TEM images of MC-2-750 are shown in Fig. 3. Particles around 50 nm are found in the carbon composites (Fig. 3(a)), and carbon coating shells on the magnetic particles are clear form the image of higher magnification (Fig. 3(b)). Near complete carbon shells formed around most magnetic particles. Such carbon shells would be helpful to improve the acid resistance of the magnetic carbon composites as confirmed by an acid resistance experiment (see below).

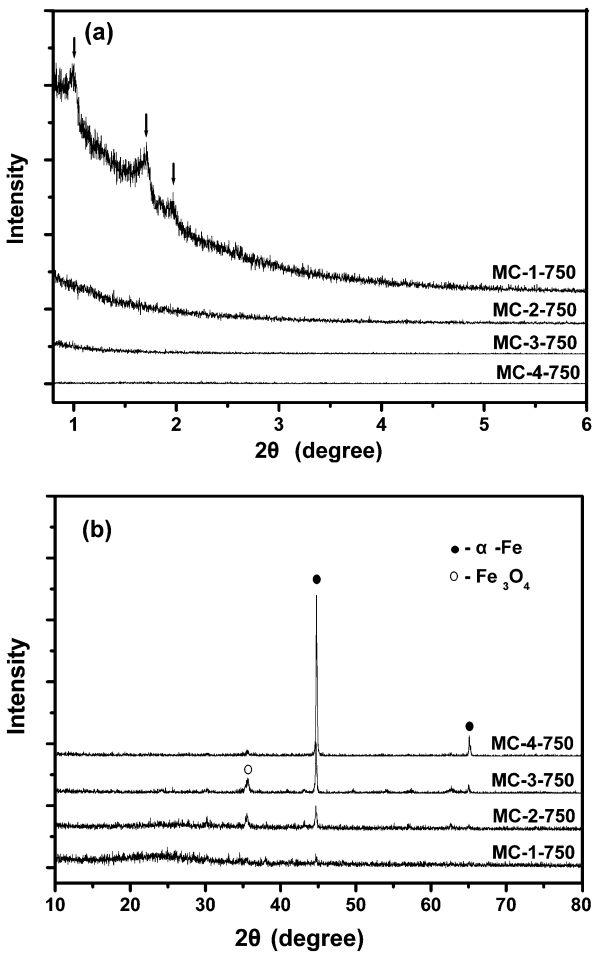

Fig. 2 Low- (a) and high-angle (b) XRD patterns of magnetic mesoporous carbon composites.

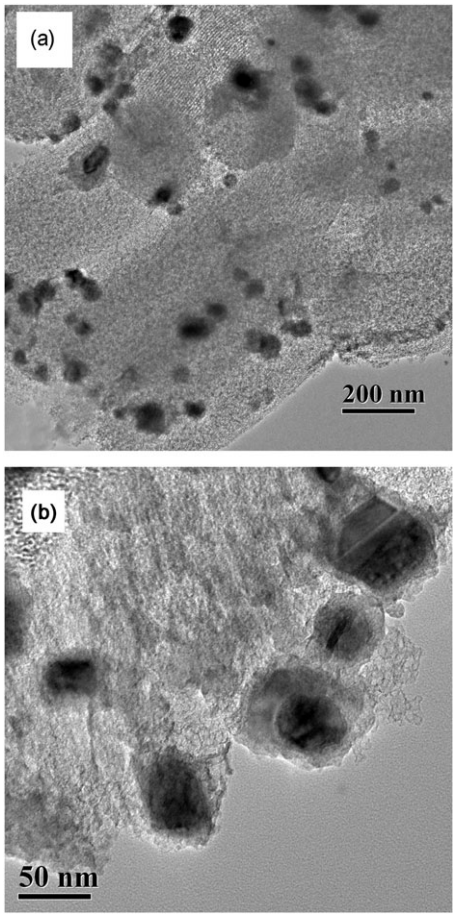

Fig. 3 TEM images of sample MC-2-750 at different magnifications showing the presence of magnetic particles of tens of nanometers in diameter on the mesoporous carbon surface (a) and the carbon shell coating on the magnetic particles (b).

Nitrogen sorption isotherms were recorded to investigate the effect of the magnetic content on the pore properties of the samples. Fig. 4(a) shows the nitrogen sorption isotherms of MC-1-750, MC-2-750, MC-3-750 and MC-4-750. All isotherm curves of the samples are found to be the type with a marked leap on the adsorption branch between relative pressures P/P_0 of 0.4 and 0.6, typical of mesoporous materials. This indicates that the mesostructure of the carbon composites has been retained after incorporating the magnetic particles; further large surface areas are also retained. The surface area (Table 1) is found to decrease gradually from MC-1-750 to MC-4-750, and similarly, the pore volume also decreases in the same order. The main reason for such decreases can be attributed to the number of magnetic particles such as α-Fe, and their much higher density than carbon. However, similar pore size distributions for all the carbon composites, in a range of 3–4.5 nm, are observed (Fig. 4(b) and Table 1).

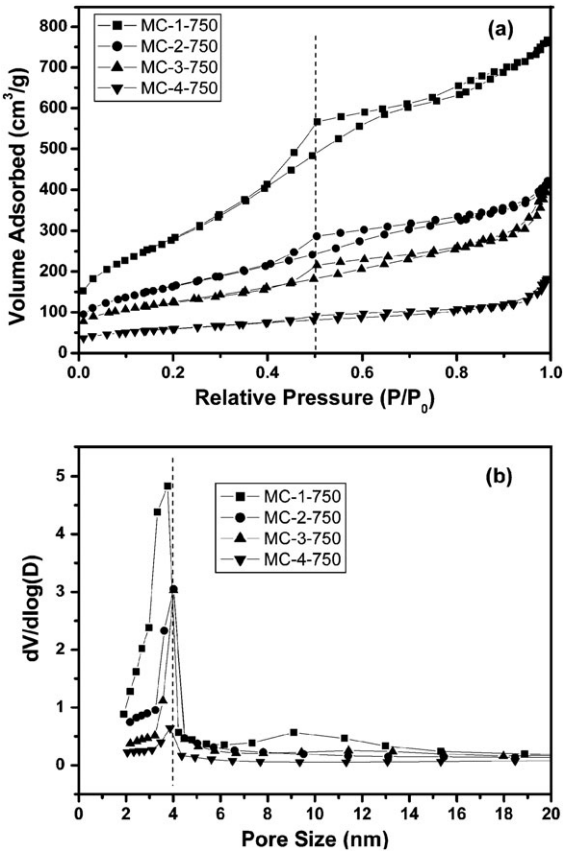

Fig. 4 (a) Nitrogen sorption isotherms and (b) the corresponding pore size distribution for magnetic mesoporous carbon composites.

We also prepared a series of samples at different carbonization temperatures to study the influence of temperature. Fig. 5 shows the high-angle XRD patterns of corresponding samples. Besides amorphous carbon, the talasspite ($Fe_3(SiO_4)_2$) phase was present when carbonization was carried out at 700 °C. With an increase of the carbonization temperature, α-Fe and Fe_3O_4 dominate at 750, 800 and 850 °C. Because one can not distinguish between the γ-Fe_2O_3 and Fe_3O_4 phases from XRD patterns, room-temperature Mössbauer spectroscopy was further used to distinguish the different magnetic iron oxides. Fig. 6 shows the Mössbauer spectrum of R-3-700, and the upper part of Fig. 6 is the simulation. Since two doublets are present in the Mössbauer spectrum, the iron compound has two iron substructures corresponding to Fe^{2+} and Fe^{3+} of talasspite and the results further confirm that the phase is talasspite ($Fe_3(SiO_4)_2$) rather than fayalite (Fe_2SiO_4). Fig. 7 shows the Mössbauer spectrum of MC-3-750, and the upper part of Fig. 7 is the simulation. The spectra could be well reproduced by assuming three sets of signals, which could be attributed to α-Fe, Fe_3O_4 and α-Fe_2O_3. The IS (isomer shifts)

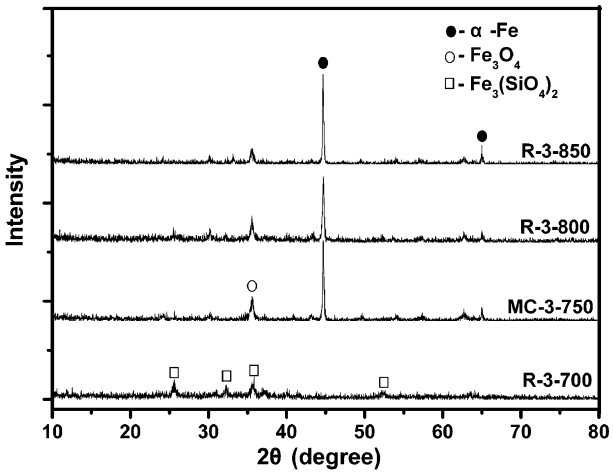

Fig. 5 The high-angle XRD patterns of the composites carbonized at different temperatures.

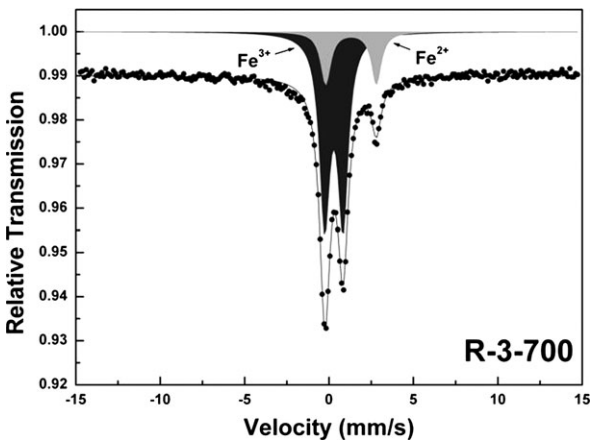

Fig. 6 Mössbauer spectrum of R-3-700 at room temperature.

and *H* (hyperfine fields) values of 0.33 mm s^{-1} and 518 KOe are for α-Fe_2O_3, while those of 0.24 mm s^{-1} and 494 KOe correspond to tetrahedral site Fe^{3+} ion and those of 0.65 mm s^{-1} and 457 KOe are for an average oxidation state of $Fe^{2.5+}$ of Fe_3O_4, respectively. From Fig. 7 it can be seen that these values are in good agreement with the literature.[33–37] The very broad peak of the top curve can be related to some amorphous phases and broad particle size distribution of iron oxide,[33] and the doublet of the top second curve may be attributed to high-spin Fe^{3+} of some amorphous hematite in an octahedral oxygen environment.[38] Here, the small quantity of α-Fe_2O_3 in samples results from the partial oxidation of α-Fe due to the small amount of magnetic particles not completely covered by a carbon shell. In order to further confirm the phase change along with the increase of carbonization temperature, the

Table 1 Pore structure parameters of the magnetic mesoporous carbon composites

Sample	BET surface area/m^2 g^{-1}	Pore volume/cm^3 g^{-1}	Pore size/nm
MC-1-750	1026.5	1.26	3.33
MC-2-750	592.7	0.71	4.01
MC-3-750	452.2	0.60	4.02
MC-4-750	211.4	0.27	3.87

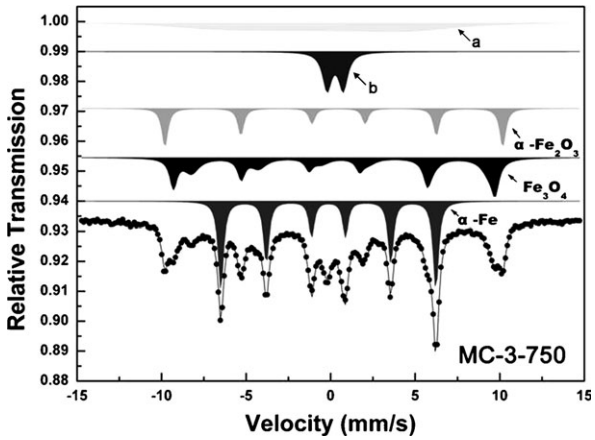

Fig. 7 Mössbauer spectrum of MC-3-750 at room temperature, the broad peak of the top curve (a) arises from the wide size distribution of iron oxide particles and some amorphous phases, the doublet (b) is for Fe^{3+} of amorphous hematite.

Mössbauer spectrum of R-3-850 was also examined (see Fig. S1, ESI†). A similar spectrum to that of MC-3-750 was obtained, which means the phase compositions containing iron did not change significantly during the carbonization from 750 to 850 °C. According to the XRD patterns and Mössbauer spectra, 750 °C is thus a high enough temperature to obtain the desired magnetic mesoporous carbon composites.

3.2 Magnetic properties of the magnetic mesoporous carbon composites and acid resistance

To test the acid resistance of the magnetic mesoporous carbon composites, 0.2 g MC-2-750 were stored in 200 mL of HCl solution (pH = 1) for 10 days. After filtration, washing with distilled water and ethanol, and drying, the acid-treated sample was denoted as MC-2-750-a. Fig. 8(a) shows the high-angle XRD patterns of MC-2-750 and MC-2-750-a. After acid-treatment, the high-angle characteristic peaks showed no apparent change. It can thus be deduced that most magnetic particles are well protected by the coating carbon shells. The magnetic separability of MC-2-750-a was demonstrated in ethanol by placing a magnet beside a glass bottle containing the sample in ethanol (Fig. 8(b)). The black particles were attracted to the magnet within a short time indicating that even a lengthy acid treatment does not show a strong influence on the magnetic performance. In order to get exact saturation magnetization strength, the magnetization curves of MC-2-750 and MC-2-750-a were also examined (Fig. 8(c)). The saturation magnetization values were 14.4 and 11.5 emu g^{-1} for MC-2-750 and MC-2-750-a, respectively. The retention of about 80% of the corresponding saturation magnetization strength indicates the good acid-resistance property of the sample.

The magnetic properties of MC-1-750, MC-3-750 and MC-4-750 were also examined (Fig. S2 and S3, ESI†), and the corresponding saturation magnetization strengths of MC-1-750, MC-3-750 and MC-4-750 are 2.8, 50.1 and 111.5 emu g^{-1}, respectively. The magnetic properties of MC-1-750, MC-2-750, MC-3-750 and MC-4-750 show soft ferromagnetism due to the much larger magnetic particle sizes

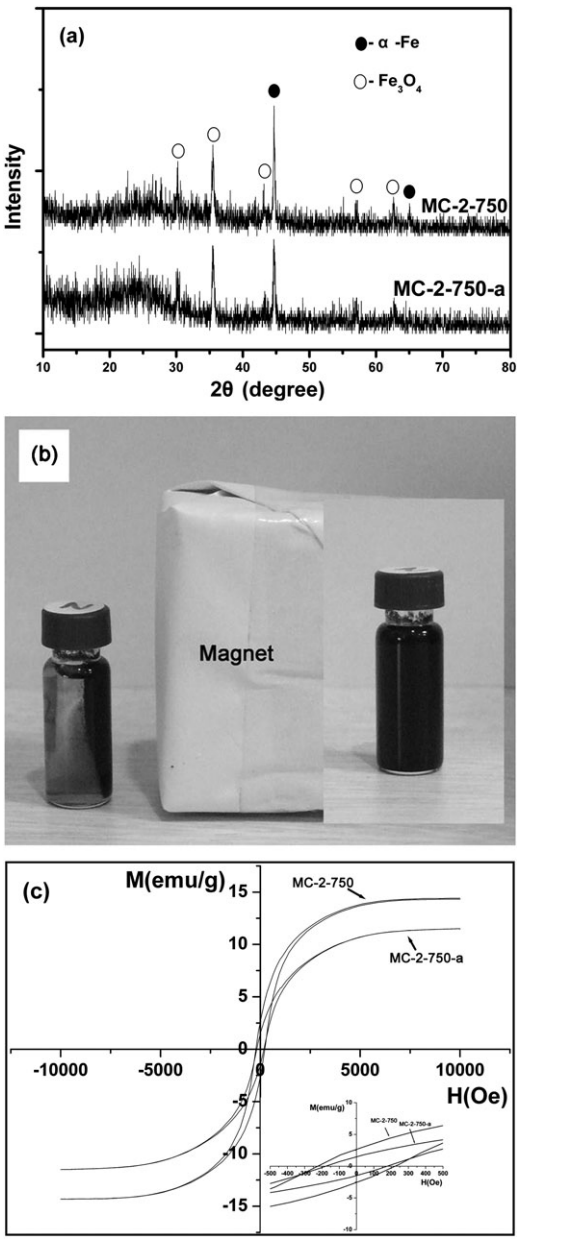

Fig. 8 (a) High-angle XRD patterns of MC-2-750 and MC-2-750-a. (b) Photograph of dispersed MC-2-750-a in ethanol before (right) and after (left) being attracted by a magnet and (c) magnetization curves of MC-2-750 and MC-2-750-a.

at increased amount of iron source added. Here, the coercivity and remanence of these samples are below 250 Oe and 5 emu g^{-1}, respectively.

4. Conclusions

In summary, we have designed and synthesized magnetically separable mesoporous carbon composites with carbon-coated magnetic particles integrated onto the mesoporous carbon particle surface by an easy co-casting method. The magnetic mesoporous carbon composites have a high surface area and sharp pore distribution. Further, the magnetic properties of the composites can be easily tuned by changing the added

amount of iron nitrate during synthesis. Furthermore, the composites show good acid resistance due to a carbon shell coating structure around the magnetic particles. The present synthesized composites combine the advantages of the mesoporous structure of the carbon, tunable magnetic susceptibility and easy magnetic separability, and good resistance against acid attack, and therefore are promising for future applications in fields such as adsorption–separation, magnetically separable catalysis, and so on.

Acknowledgements

The authors gratefully acknowledge the support of this research by the National Science Foundation of China Research (Grant No. 50702072 and 20633090), National 863 plans projects (Grant No. 2007AA03Z317), Chinese Academy of Science (Grant No. KJCX2.YW.MO2 and KJCX2-YW-210), and Shanghai Nano-Science Program (Grant No. 0852nm03900).

References

1 (*a*) Z. Wu, Y. Yang, D. Gu, Y. Zhai, D. Feng, Q. Li, B. Tu, P. Webley and D. Zhao, *Top. Catal.*, 2009, **52**, 12; (*b*) X. Zhang, F. Zhang, X. Yan, Z. Zhang, F. Sun, Z. Wang and D. Zhao, *J. Porous Mater.*, 2008, **15**, 145; (*c*) Z. Luan, E. Maes, H. Van der, D. Zhao, R. Czernuszewicz and L. Kevan, *Chem. Mater.*, 1999, **11**, 3680; (*d*) J. Zhao, B. Tian, Y. Yue, W. Hua, D. Zhao and Z. Gao, *J. Mol. Catal. A: Chem.*, 2005, **242**, 218; (*e*) W. Dong, Y. Sun, C. Lee, W. Hua, X. Lu, Y. Shi, S. Zhang, J. Chen and D. Zhao, *J. Am. Chem. Soc.*, 2007, **129**, 13894; (*f*) Y. Liu, J. Xu, L. He, Y. Cao, H. He, D. Zhao, J. Zhuang and K. Fan, *J. Phys. Chem. C*, 2008, **112**, 16575.
2 (*a*) X. Dong, W. Shen, Y. Zhu, L. Xiong and J. Shi, *Adv. Funct. Mater.*, 2005, **15**, 955; (*b*) L. Li, J. Shi, L. Zhang, L. Xiong and J. Yan, *Adv. Mater.*, 2004, **16**, 1079; (*c*) C. Yu, X. Dong, L. Guo, J. Li, F. Qin, L. Zhang, J. Shi and D. Yan, *J. Phys. Chem. C*, 2008, **112**, 13378; (*d*) L. Li and J. Shi, *Adv. Synth. Catal.*, 2008, **350**, 667; (*e*) L. Li and J. Shi, *Chem. Commun.*, 2008, 996.
3 S. Nguyen, V. Szabo, D. Trong On and S. Kaliaguine, *Microporous Mesoporous Mater.*, 2002, **54**, 51.
4 L. Chen, J. Hu and R. Richards, *J. Am. Chem. Soc.*, 2009, **131**, 914.
5 K. Nakajima, M. Okamura, J. Kondo, K. Domen, T. Tatsumi, S. Hayashi and M. Hara, *Chem. Mater.*, 2009, **21**, 186.
6 J. Zhou, J. He, T. Wang, D. Sun, G. Zhao, X. Chen, X. D. Wang and Z. Di, *J. Mater. Chem.*, 2008, **18**, 47.
7 H. Zhao, M. Kayser, Y. Wang, R. Palkovits and F. Schüth, *Microporous Mesoporous Mater.*, 2008, **116**, 196.
8 J. Li, S. Liu, Y. He and J. Wang, *Microporous Mesoporous Mater.*, 2008, **115**, 416.
9 (*a*) C. Kresge, M. Leonowicz, W. Roth, J. Vartuli and J. Beck, *Nature*, 1992, **359**, 710; (*b*) J. Vartuli, K. Schmitt, C. Kresge, W. Roth, M. Leonowicz, S. McCullen, S. Hellring, J. Beck, J. Schlenker, D. Olson and E. Sheppard, *Chem. Mater.*, 1994, **6**, 2317.
10 A. Corma, *Chem. Rev.*, 1997, **97**, 2373.
11 (*a*) D. Zhao, J. Feng, Q. Huo, N. Melosh, G. Fredrickson, B. Chmelka and G. Stucky, *Science*, 1998, **279**, 548; (*b*) Y. Wan and D. Zhao, *Chem. Rev.*, 2007, **107**, 2821.
12 F. Kleitz, S. Hei and R. Ryoo, *Chem. Commun.*, 2003, 2136.
13 Y. Li, J. Shi, Z. Hua, H. Chen, M. Ruan and D. Yan, *Nano Lett.*, 2003, **3**, 609.
14 G. Büchel, K. Unger, A. Matsumoto and K. Tsutsumi, *Adv. Mater.*, 1998, **10**, 1036.
15 A. Lu and F. Schüth, *Adv. Mater.*, 2006, **18**, 1793.
16 M. Tiemann, *Chem. Mater.*, 2008, **20**, 961.
17 C. Liang, Z. Li and S. Dai, *Angew. Chem., Int. Ed.*, 2008, **47**, 3696.
18 (*a*) R. Ryoo, S. Joo and S. Jun, *J. Phys. Chem. B*, 1999, **103**, 7743; (*b*) M. Kruk, M. Jaroniec and R. Ryoo, *Chem. Mater.*, 2000, **12**, 1414; (*c*) S. Joo, S. Choi, I. Oh, J. Kwak, Z. Liu, O. Terasaki and R. Ryoo, *Nature*, 2001, **412**, 169; (*d*) T. Kim, I. Park and R. Ryoo, *Angew. Chem., Int. Ed.*, 2003, **42**, 4375.
19 (*a*) Z. Li, W. Yan and S. Dai, *Langmuir*, 2005, **21**, 11999; (*b*) Z. J. Li and S. Dai, *Chem. Mater.*, 2005, **17**, 1717.
20 (*a*) Y. Xia and R. Mokaya, *Adv. Mater.*, 2004, **16**, 886; (*b*) Y. Xia and R. Mokaya, *Chem. Mater.*, 2005, **17**, 1553.
21 X. Liu, B. Tian, Z. Yu, F. Gao, S. Xie, B. Tu, R. Che, L. Peng and D. Zhao, *Angew. Chem., Int. Ed.*, 2002, **41**, 3876.
22 C. Liang, K. Hong, G. Guiochon, J. Mays and S. Dai, *Angew. Chem., Int. Ed.*, 2004, **43**, 5785.
23 (*a*) F. Zhang, Y. Meng, D. Gu, Y. Yan, C. Yu, B. Tu and D. Zhao, *J. Am. Chem. Soc.*, 2005, **127**, 13508; (*b*) Y. Meng, D. Gu, F. Zhang, Y. Shi, L. Cheng, D. Feng, Z. Wu, Z. Chen, Y. Wan, A. Stein and D. Zhao, *Chem. Mater.*, 2006, **18**, 4447; (*c*) Y. Meng, D. Gu, F. Zhang, Y. Shi, H. Yang, Z. Li, C. Yu, B. Tu and D. Zhao, *Angew. Chem., Int. Ed.*, 2005, **44**, 7053; (*d*) F. Zhang, Y. Meng, D. Gu, Y. Yan, Z. Chen, B. Tu and D. Zhao, *Chem. Mater.*, 2006, **18**, 5279.
24 Y. Zhu, L. Zhang, F. Schappacher, R. Pöttgen, J. Shi and S. Kaskel, *J. Phys. Chem. C*, 2008, **112**, 8623.
25 (*a*) M. Hartmann, A. Vinu and G. Chandrasekar, *Chem. Mater.*, 2005, **17**, 829; (*b*) A. Vinu, K. Hossain, G. Kumar and K. Ariga, *Carbon*, 2006, **44**, 530; (*c*) A. Vinu, M. Miyahara and K. Ariga, *J. Phys. Chem. B*, 2005, **109**, 6436.
26 X. Zhuang, Y. Wan, C. Feng, Y. Shen and D. Zhao, *Chem. Mater.*, 2009, **21**, 706.
27 A. Lu, W. Li, A. Kiefer, W. Schmidt, E. Bill, G. Fink and F. Schüth, *J. Am. Chem. Soc.*, 2004, **126**, 8616.
28 (*a*) Z. Guo, L. Henry and E. Podlaha, *ECS Trans.*, 2006, **1**, 63; (*b*) Z. Guo, S. Park and H. Hahn, *Appl. Phys. Lett.*, 2007, **90**, 053111.
29 (*a*) A. Lu, W. Li, N. Matoussevitch, B. Spliethoff, H. Bönnemann and F. Schüth, *Chem. Commun.*, 2005, 98; (*b*) A. Lu, W. Schmidt, N. Matoussevitch, H. Bönnemann, B. Spliethoff, B. Tesche, E. Bill, W. Kiefer and F. Schüth, *Angew. Chem., Int. Ed.*, 2004, **43**, 4303.
30 (*a*) A. Fuertes and P. Tartaj, *Chem. Mater.*, 2006, **18**, 1675; (*b*) A. Fuertes and P. Tartaj, *Small*, **3**, 275; (*c*) A. Fuertes, T. Valds-Sols, M. Sevilla and P. Tartaj, *J. Phys. Chem. C*, 2008, **112**, 3648.
31 J. Lee, S. Jin, Y. Hwang, J. Park, H. Park and T. Hyeon, *Carbon*, 2005, **43**, 2536.
32 I. Park, M. Choi, T. Kim and R. Ryoo, *J. Mater. Chem.*, 2006, **16**, 3409.
33 X. Dong, H. Chen, W. Zhao, X. Li and J. Shi, *Chem. Mater.*, 2007, **19**, 3484.
34 R. Bauminger, S. Cohen, A. Marinov, S. Ofer and E. Segal, *Phys. Rev.*, 1961, **122**, 1447.
35 R. Armstrong, A. Morrish and G. Sawatzky, *Phys. Lett.*, 1966, **23**, 414.
36 M. Pérez-Cabero, J. Taboaba, A. Guerrero-Ruiz, A. Overweg and I. Rodríguez-Ramos, *Phys. Chem. Chem. Phys.*, 2006, **8**, 1230.
37 F. Jiao, J. Jumas, M. Womes, A. Chadwick, A. Harrison and P. Bruce, *J. Am. Chem. Soc.*, 2006, **128**, 12905.
38 F. Jiao, A. Harrison, J. Jumas, A. Chadwich, W. Kocheimann and P. Bruce, *J. Am. Chem. Soc.*, 2006, **128**, 5468.